Since January 2020 Elsevier has created a COVID-19 resource centre with free information in English and Mandarin on the novel coronavirus COVID-19. The COVID-19 resource centre is hosted on Elsevier Connect, the company's public news and information website.

Research Article

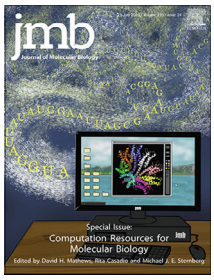

The RNA Interference Effector Protein Argonaute 2 Functions as a Restriction Factor Against SARS-CoV-2

Joaquin Lopez-Orozco [1†], Nawell Fayad [1†], Juveriya Qamar Khan [3], Alberto Felix-Lopez [2], Mohamed Elaish [1], Megha Rohamare [3], Maansi Sharma [3], Darryl Falzarano [4,5], Jerry Pelletier [6], Joyce Wilson [3], Tom C. Hobman [1,2,7*] and Anil Kumar [3*]

*1 - **Department of Cell Biology,** Faculty of Medicine & Dentistry, University of Alberta, Edmonton, Canada*
*2 - **Department of Medical Microbiology & Immunology,** Faculty of Medicine & Dentistry, University of Alberta, Edmonton, Canada*
*3 - **Department of Biochemistry,** Microbiology and Immunology, University of Saskatchewan, Saskatoon, Canada*
*4 - **Vaccine and Infectious Disease Organization (VIDO),** University of Saskatchewan, Saskatoon, Canada*
*5 - **Department of Veterinary Microbiology,** University of Saskatchewan, Saskatoon, Canada*
*6 - **Department of Biochemistry,** McGill University, Montreal, Canada*
*7 - **Li Ka Shing Institute of Virology,** University of Alberta, Edmonton, Canada*

Correspondence to Tom C. Hobman and Anil Kumar: *Corresponding authors. tom.hobman@ualberta.ca (T.C. Hobman), anil.kumar@usask.ca (A. Kumar)*
https://doi.org/10.1016/j.jmb.2023.168170
Edited by Leslie Parent

Abstract

Argonaute 2 (Ago2) is a key component of the RNA interference (RNAi) pathway, a gene-regulatory system that is present in most eukaryotes. Ago2 uses microRNAs (miRNAs) and small interfering RNAs (siRNAs) for targeting to homologous mRNAs which are then degraded or translationally suppressed. In plants and invertebrates, the RNAi pathway has well-described roles in antiviral defense, but its function in limiting viral infections in mammalian cells is less well understood. Here, we examined the role of Ago2 in replication of the betacoronavirus SARS-CoV-2, the etiologic agent of COVID-19. Microscopic analyses of infected cells revealed that a pool of Ago2 closely associates with viral replication sites and gene ablation studies showed that loss of Ago2 resulted in over 1,000-fold increase in peak viral titers. Replication of the alphacoronavirus 229E was also significantly increased in cells lacking Ago2. The antiviral activity of Ago2 was dependent on both its ability to bind small RNAs and its endonuclease function. Interestingly, in cells lacking Dicer, an upstream component of the RNAi pathway, viral replication was the same as in parental cells. This suggests that the antiviral activity of Ago2 is independent of Dicer processed miRNAs. Deep sequencing of infected cells by other groups identified several SARS-CoV-2-derived small RNAs that bind to Ago2. A mutant virus lacking the most abundant ORF7A-derived viral miRNA was found to be significantly less sensitive to Ago2-mediated restriction. This combined with our findings that endonuclease and small RNA-binding functions of Ago2 are required for its antiviral function, suggests that Ago2-small viral RNA complexes target nascent viral RNA produced at replication sites for cleavage. Further studies are required to elucidate the processing mechanism of the viral small RNAs that are used by Ago2 to limit coronavirus replication.

Please cite tts article as: J. Lopez-Orozco, N. Fayad, J.Q. Khan, et al., The RNA Interference Effector Protein Argonaute 2 Functions as a Restriction Factor Against SARS-CoV-2Journal of Molecular Biology, https://doi.org/10.1016/j.jmb.2023.168170

Introduction

Severe acute respiratory syndrome coronavirus 2 (SARS-CoV-2) is the etiologic agent of COVID-19,[1] an infectious disease that has resulted in millions of deaths across the globe over the past 3 years. This betacoronavirus is transmitted with high efficiency primarily through respiratory aerosols between humans and rapidly establishes infection shortly after exposure.[2–4] Fortunately, the development of vaccines and direct-acting antivirals (reviewed in[5,6]) has reduced the burden of disease in many countries. However, with the continuous emergence of variants of concern, the effectiveness of current vaccines and monoclonal antibodies that were designed against earlier strains of SARS-CoV-2, are significantly lower (reviewed in[7,8]). To identify novel targets for antiviral therapy, considerable efforts have been devoted to understanding how SARS-CoV-2 affects host cell pathways during infection. For example, an interactome screen by Gordon et al identified multiple virus-host protein interactions that could be targeted pharmacologically.[9] In addition, other interactome studies and CRISPR screens have identified both host restriction and dependency factors that function to inhibit or support SARS-CoV-2 replication.[10,11] Ultimately, stockpiling a battery of drugs that target viral proteins as well as host dependency and restriction factors will leave us better prepared for future pandemics.[12]

The interferon (IFN) system is a critical arm of the innate immune response that functions to restrict replication of viruses that infect mammalian cells. SARS-CoV-2 is particularly sensitive to these cytokines[13] which is likely why this virus has evolved many mechanisms to interfere with IFN induction and signaling.[14] In addition to the IFN response, the RNA interference (RNAi) pathway which uses small RNAs to regulate gene expression at the post-transcriptional level,[15] is critical for blocking replication of viruses in plants and other lower eukaryotes that lack an IFN system.[16–19] However, whereas multiple studies suggest that RNA-based gene-silencing also plays an important antiviral role in mammalian cells[20–23] others indicate a proviral role for Argonaute (Ago) proteins,[24–26] which are the main effectors of RNAi. Ago proteins use small RNAs to silence homologous mRNAs by translational suppression or endonuclease-mediated cleavage. Among the four Ago proteins expressed in mammalian cells, only Ago2 possesses endonuclease activity.[27,28] Here, we show that Ago2 is a restriction factor for SARS-CoV-2. In infected cells, a pool of Ago2 localized in close proximity to viral replication sites. SARS-CoV-2 genomic RNA levels and viral titers were increased more than 1,000-fold in cells lacking *Ago2*. Mutational analyses revealed that the endonuclease activity and small RNA binding ability of Ago2 are important for its antiviral function. Reverse genetics studies suggest that viral transcript derived small RNAs play an essential role in Ago2-mediated restriction of SARS-CoV-2. Finally, Ago2 appears to be a pan-coronavirus restriction factor as it was found to limit replication of both alpha- and betacoronaviruses.

Results

SARS-CoV2 infection disrupts localization of Ago2

Ago2 associates with a variety of cytoplasmic ribonucleoprotein complexes including processing bodies (P-bodies) and stress granules (SG).[29,30] Here, we examined whether association of Ago2 to these ribonucleoprotein complexes was perturbed in the context of infection. To study SARS-CoV-2 infection in lung cells,[31] we used a human lung epithelial H23 cell line engineered to overexpress the SARS-CoV-2 entry receptor Angiotensin-Converting Enzyme 2 (ACE2) (H23-ACE2).[32] SG formation was triggered by inducing oxidative stress using sodium arsenite[33] or translational stress using the polyhydroxysteroid, hippuristanol, which blocks the helicase activity of eukaryotic initiation factor 4A.[34] Compared to uninfected cells treated with DMSO only, stressed H23-ACE2 cells contained dense cytosolic aggregates that co-stained with antibodies to the SG marker TIA1 as well as Ago2 (Figure 1(A)). SGs were significantly lower in SARS-CoV-2 infected cells regardless of whether they were stressed with arsenite or hippuristanol (Figure 1(A-B)). Similarly, SARS-CoV-2 infection resulted in a significant loss of p-bodies labeled with the markers GW182[35,36] or Dcp1a (Figures 2(A-B) and Figure S1(A-D)). Specifically, both GW182-positive puncta as well as puncta double positive for GW182 and Ago2 were reduced following infection (Figure 2(A-B), Figure S1(A)). Granules positive for Ago2 alone were significantly lower in SARS-CoV-2 infected cells but remain at higher counts than GW+Ago2+ bodies and suggest a novel localization of Ago2 loci that is unrelated to p-bodies (Figure S1(B)). Despite this change in counts of granule-like Ago2, it is important to note that both mock and infected H23-ACE2 cells expressed similar levels of Ago2 protein (Figure S3(A)). Taken together, these data suggest that SARS-CoV-2 infection affects formation and/or stability of multiple ribonucleoprotein complexes such as SGs and P-Bodies, which is in agreement with a recently published report.[37–40]

Ago2 localizes to puncta that associate with SARS-CoV-2 replication complexes

Following SARS-CoV-2 infection, Ago2-containing puncta that do not contain the canonical P-body markers Dcp1a (Figure 3(A)) or GW182 (S1B) remain. Many of these Ago2-positive structures were in close proximity to virus

replication sites as defined by the presence of double-strand RNA (Figure 3(A-B(and Figure S2 (A)). Moreover, colocalization analysis showed that ~12% of dsRNA foci co-localized with Ago2-positive puncta which did not contain Dcp1a (Figure 3(B)) and therefore were not P-bodies. A

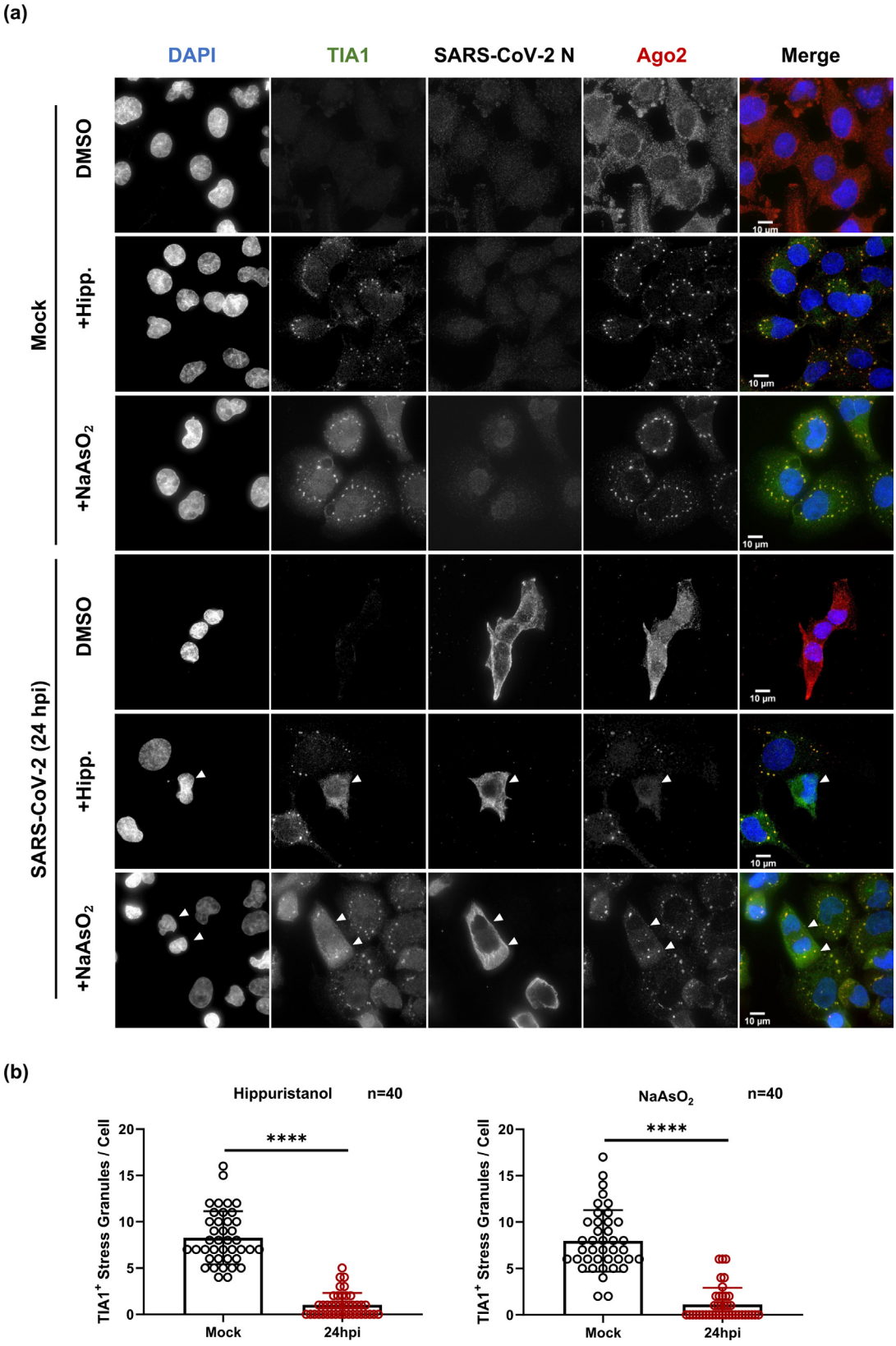

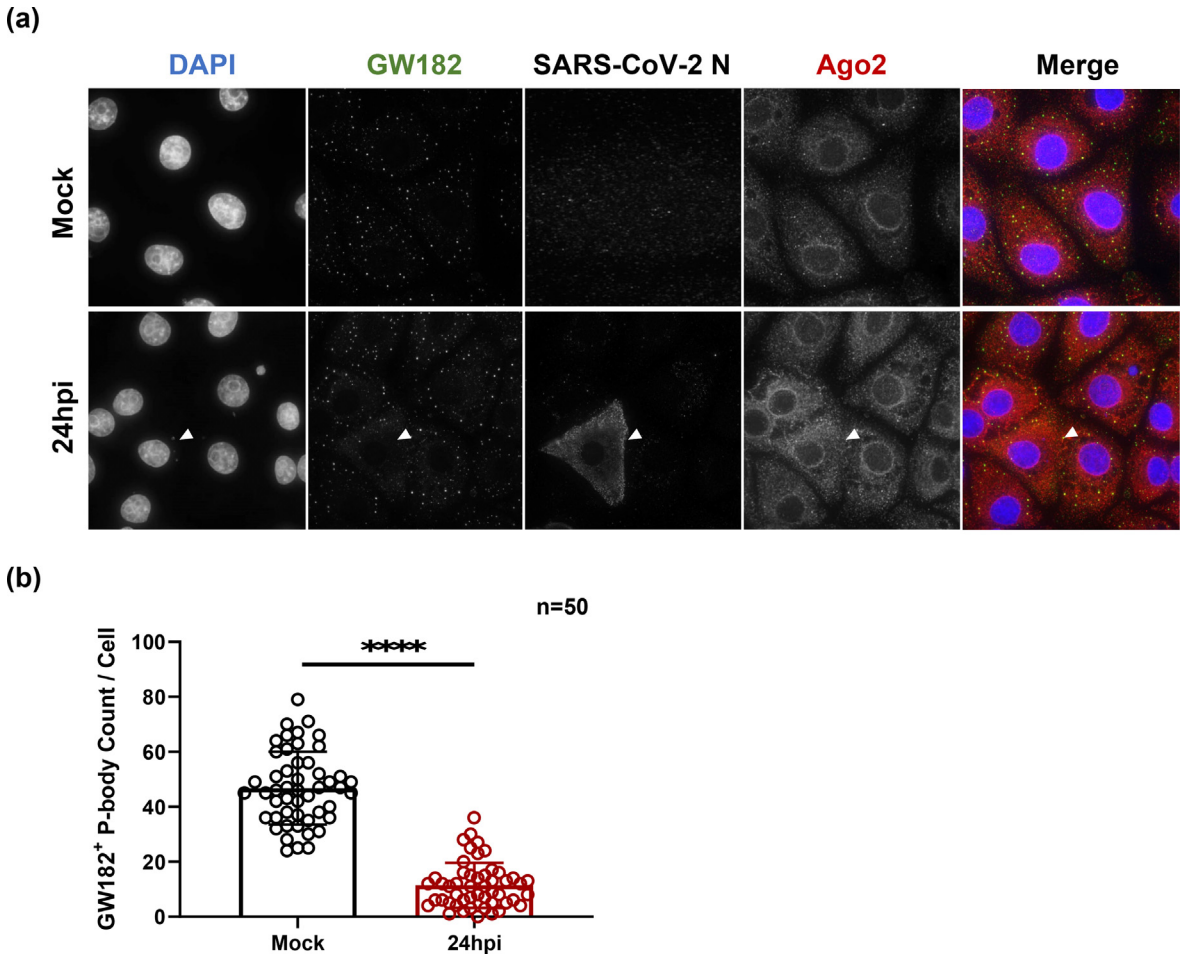

Figure 2. SARS-CoV-2 infection disrupts the assembly of Ago2-associated P-bodies. (a) A549-ACE2 cells were infected with SARS-CoV-2 (VIDO 01; [MOI] = 0.5). After fixation, cells were immunolabeled with anti-GW182 in green (P-body marker), anti-SARS-CoV-2 nucleocapsid (N; not included in merge), and anti-Ago2 in red. DAPI in blue was used as a nuclear counterstain. Infected cells are highlighted with white arrow heads. (b) GW182 + P-bodies were counted on a per cell basis using Volocity software. A total of 50 cells were counted for each condition from 3 biological replicates. Cells were imaged at 60X on a Deltavision Elite deconvolution microscope. Values expressed as mean ± standard deviation (****$p \leq 0.0001$). Unpaired t-tests were performed for statistical analysis.

similar close localization of Ago2 and dsRNA was observed in cells infected with the alphacoronavirus 229E (Figure S4). Given that a pool of Ago2 localizes to virus replication sites we next examined if/how Ago2 expression affected viral RNA replication.

Cells lacking Ago2 are more permissive for SARS-CoV-2 replication

To determine how Ago2 affects virus replication, we employed an *Ago2* knockout (KO) cell line that was produced by CRISPR gene ablation.[41] Immunoblotting confirmed that Ago2 protein was not

Figure 1. Ago2-associated stress granule assembly is disrupted during SARS-CoV-2 infection. (a) H23-ACE2 cells infected with SARS-CoV-2 (VIDO 01; multiplicity of infection [MOI] = 0.5) were fixed 24 h post-infection (hpi). Uninfected and untreated (Mock and DMSO) cells were included as controls. Thirty minutes prior to fixation, cells were treated with either 1 μM hippuristanol (Hipp.) or 500 μM sodium arsenite ($NaAsO_2$) to trigger stress granule assembly by two different mechanisms. Cells were immunolabeled with anti-TIA1 in green (stress granule marker), anti-SARS-CoV-2 nucleocapsid (N; not included in merge), and anti-Ago2 in red. DAPI in blue was used as a nuclear counterstain. Infected cells are highlighted with white arrow heads. (b) TIA1 + stress granules were counted on a per cell basis using Volocity software. A total of 40 cells were counted for each condition from 3 biological replicates. Cells were imaged at 60X on a Deltavision Elite deconvolution microscope. Values expressed as mean ± standard deviation (****$p \leq 0.0001$). Unpaired t-tests were performed for statistical analysis.

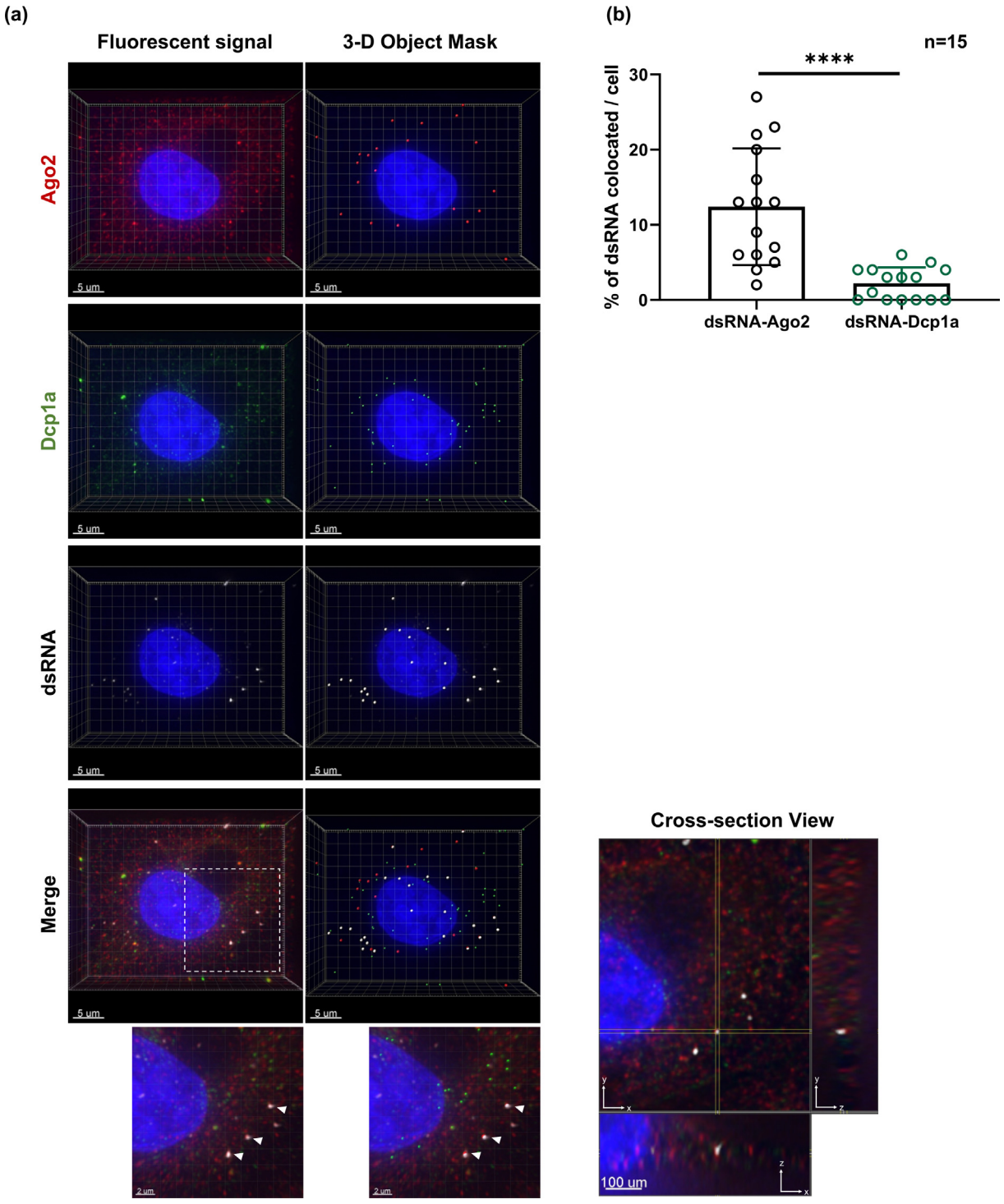

Figure 3. Ago2 localizes near SARS-CoV-2 replication complexes. (a) A549-ACE2 cells infected with SARS-CoV-2 (VIDO 01; [MOI] = 0.5) were fixed 24 hpi. Cells were immunolabeled with anti-dsRNA in white (marker of SARS-CoV-2 replication complexes), anti-Ago2 in red, and anti-Dcp1a in green. 3-D objects were created for each channel in Imaris software based on specified thresholds for size and fluorescent intensity. The dashed box is the area shown in the high magnification insets and cross-section view showing dsRNA colocalizing with Ago2 (highlighted with white arrow heads). DAPI in blue was used as a nuclear counterstain. (b) dsRNA co-locating to Ago2 or Dcp1a (within 0.5 um or less of each other) 3-D objects were counted on a per cell basis. A total of 15 cells were counted for 3 biological replicates. Cells were imaged at 60X on a Deltavision Elite deconvolution microscope. Values expressed as mean ± standard deviation (****$p \leq 0.0001$). Unpaired t-tests were performed for statistical analysis.

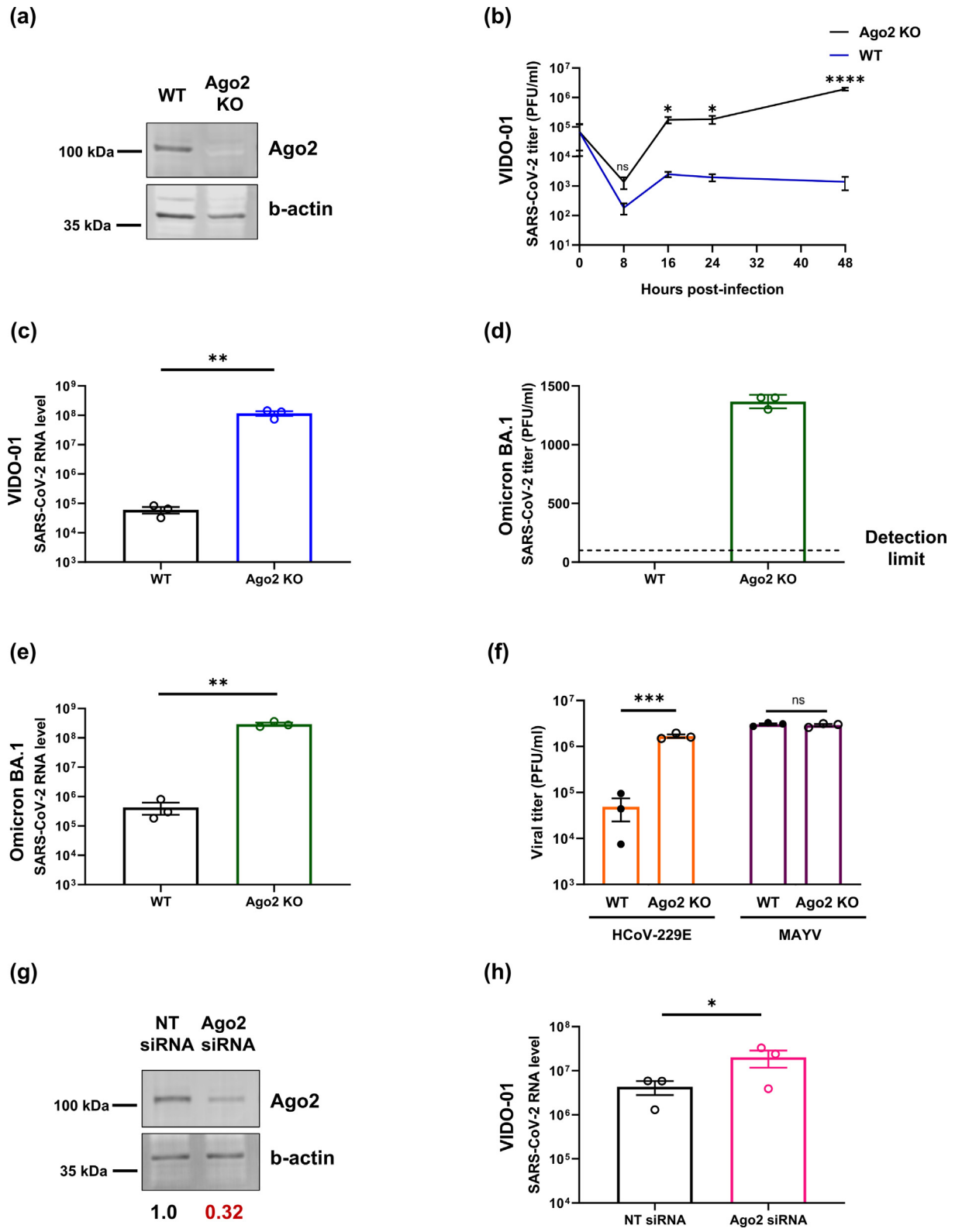

detected in the Huh7.5 Ago2 KO cells (Figure 4(A)). Parental Huh7.5 cells and *Ago2* KO cells were infected with a Wuhan-like strain of SARS-CoV-2 (VIDO-01)[14] and viral titers in the cell media collected at multiple time points post-infection, were determined by plaque assay. In the absence of Ago2, SARS-CoV-2 replicated to significantly higher viral titers from 16 h onwards, reaching up to 1,000-fold higher viral titers compared to the parental cell line at 48 h (Figure 4(B)). Similarly, levels of SARS-

CoV-2 genomic RNA were more than 1,000-fold higher in *Ago2* KO cells at 24 h post-infection (Figure 4(C)). The increase in permissiveness was not due to elevated expression of ACE2 in Huh7.5 *Ago2* KO cells (Figure S3(B)). Similar results were observed when *Ago2* KO cells were infected with a more recent strain of SARS-CoV-2, Omicron BA.1 (Figure 4(D,E)) and the alphacoronavirus HCoV-229E (Figure 4(F)). However, loss of Ago2 expression had no effect on replication of Mayaro virus, an arboviral pathogen in the family *Togaviridae* (Figure 4(F)). To rule out the possibility that the antiviral effect of Ago2 was specific to Huh7.5 cells, Calu-3 cells, a more permissive human lung adenocarcinoma line[42] were transfected with siRNAs against Ago2 or a non-targeting control 48 h prior to infection with SARS-CoV-2. Although Ago2 expression was only reduced by 68%, this was associated with a 5-fold increase in viral RNA levels (Figure 4(G,H)).

The endonuclease and RNA binding functions of Ago2 are critical for restriction of SARS-CoV-2

Next, we examined the potential mechanism by which Ago2 restricts replication of SARS-CoV-2. Because this protein is involved in miRNA-based gene-silencing, we first investigated if cellular miRNAs were required for the antiviral activity of Ago2 by infecting Huh7.5 cells lacking the endonuclease Dicer[43] with SARS-CoV-2. Immunoblotting confirmed that Dicer protein was not detected in the Huh7.5 *Dicer1* KO cells (Figure 5(A)). The processing of pre-miRNAs by Dicer is required to generate mature miRNAs that are loaded onto Argonaute proteins which then translationally suppress mRNAs. Indeed, loss of Dicer activity has been shown to reduce miRNA levels by 99.9%.[44] Interestingly, loss of Dicer expression had no effect on SARS-CoV-2 titers compared to parental Huh7.5 cells (Figure 5(B)). These data suggest that canonical miRNAs biogenesis is not required for the ability of Ago2 to restrict coronavirus replication.

To ensure that the increased replication of SARS-CoV-2 was in fact due to lack of Ago2 function *per se*, Huh7.5 *Ago2* KO cells were electroporated with plasmids encoding human Ago2 or yellow fluorescent protein (YFP) as negative control, followed by infection with SARS-CoV-2 (Figure 5(C)). Data in Figure 5(D) show that expression of Ago2 resulted in ~30-fold reduction in viral genomic RNA compared to cells expressing YFP. Conversely, expression of a mutant Ago2 that lacks endonuclease activity (H634P[27]), did not reduce SARS-CoV-2 levels (Figure 5(D)). Intriguingly, viral RNA levels appeared to be slightly higher in cells expressing a mutant of Ago2 that cannot bind small RNAs (Y529E[45,46]), although the difference was not statistically significant. Taken together, these data indicate that while the endonuclease activity of Ago2 is critical for its antiviral activity against coronaviruses, cellular miRNAs do not appear to be important for this function.

Virus derived small RNAs are used by Ago2 to target viral genome downregulation

Virus derived small RNAs (viRNAs) have been found in cells infected with a variety of viruses from diverse families.[47–51] Deep sequencing of SARS-CoV-2 infected cells identified several virus-encoded small complementary RNAs,[52–54] which could potentially act as guide strands for Ago2. While these previous studies focused on their role as miRNAs regulating cellular mRNAs, our study examined their potential role as single-stranded guides for the cleavage of viral genome by Ago2.

Figure 4. Ago2 is a SARS-CoV-2 restriction factor. (a) Cell lysates from wild-type (WT) Huh7.5 and Huh7.5 Ago2 knock-out (KO) were analyzed by immunoblotting to confirm Ago2 KO using anti-Ago2 and anti-actin antibodies. (b) Media from parental (WT) and *Ago2* KO Huh7.5 cells infected with SARS-CoV-2 VIDO-01 (MOI = 0.5) were collected at multiple timepoints and viral titers was determined using VeroCCL81 cells. (c) WT Huh7.5 and *Ago2* KO cells were infected with SARS-CoV-2 VIDO-01 (MOI = 0.5). Total RNA was harvested at 24 hpi. Viral RNA level was measured by qRT-PCR, normalized to ACTB mRNA levels, and expressed as fold values relative to mock-infected cells. (d) WT Huh7.5 and *Ago2* KO cells were infected with SARS-CoV-2 Omicron BA.1 (MOI = 0.5) and viral RNA level was measured as mentioned in c. (e) Media from WT Huh7.5 and *Ago2* KO cells infected with SARS-CoV-2 Omicron BA.1 (MOI = 0.5) were collected 24 hpi and viral titers were determined using VeroTMPRSS2 cells. (f) Media from WT Huh7.5 and *Ago2* KO cells infected with HCoV-229E or Mayaro virus (MAYV) (MOI = 0.5) and harvested 24 hpi were subjected to plaque assay to determine viral titers in Vero cells. (g) Lysates of Calu3 cells transfected with siRNAs against Ago2 or a non-targeting (NT) siRNA-control were collected 48 h post-transfection and analyzed by immunoblotting using anti-Ago2 or anti-actin antibodies. Numbers under the lanes represent Ago2 levels normalized to actin. (h) Calu3 cells were transfected with siRNAs against Ago2 or NT siRNA-control as in panel g. Cells were infected with SARS-CoV-2 VIDO-01 (MOI = 0.5) and RNA was harvested as described in c. Data in panels b, c, d, e, f and h are from 3 biological replicates. Error bars indicate the standard error of the mean (SEM). Asterisks indicate a statistically significant difference ($*p \leq 0.05$, $**p \leq 0.01$, $***p \leq 0.001$). Two-Way ANOVA and Sidak multiple comparisons tests were performed for b. Ratio paired t-tests were performed for c, e, and h. Multiple t-tests using the Holm-Sidak method were performed for f.

The most abundant viRNA reported in SARS-CoV-2 infected cells is CoV2-miR-O7a (Figure 6(A)) which is derived from the accessory gene ORF7A.[53,54] The primary sequence of CoV2-miR-O7a is highly similar among SARS-CoV-2 variants (Figure 6(B)) and its secondary hairpin-like structure is conserved among other betacoronaviruses such as the bat RaTG13 and SARS coronavirus.[53]

We used a molecular clone of SARS-CoV2 lacking the CoV2-miR-O7a to test its role in Ago2-dependant viral restriction (Figure 6(C)). Briefly, we generated molecular clones of SARS-CoV-2 Wuhan and Delta strain viruses named 'Wuhan WT' and 'Delta WT', respectively. Using the 'Wuhan WT' virus backbone we replaced the NS7A ORF with a NanoLuciferase (NLuc) sequence, to generate 'Wuhan 7A del' clone which does not express the NS7A protein, nor the CoV2-miR-O7a.[55] Lastly, a 'Delta 7A mut' that does not encode the ORF7A protein but maintains the CoV2-miR-O7a sequence was created from the 'Delta WT' virus backbone by mutating the methionine codons at amino acid positions 1 and 12 to stop codons. This virus serves as control for expression of the ORF7A protein.

Virus stocks produced from the molecular clones were verified by RNA sequencing and then used to infect parental and *Ago2* KO Huh7.5 cells. As expected, infection with Wuhan WT and Delta WT viruses produced higher titers in *Ago2* KO compared to parental Huh7.5 cells (Figure 6(D-E)). Infection of Huh7.5 cells with Wuhan 7A del virus lacking the viRNA CoV2-miR-O7a resulted in over 100-fold increase in viral titers compared to Wuhan WT, which was comparable to what was observed in *Ago2* KO cells infected with Wuhan WT. Wuhan 7A del virus showed significantly higher titers compared to Wuhan WT regardless of cell background (Figure 6(D)). To test the contribution of OFR7A protein to this process, we compared the replication of Delta 7A mut (lacking ORF7A protein expression but not CoV2-miR-O7a) with Delta WT. Data in Figure 6(E) shows that viral titers of 'Delta WT' and 'Delta 7A mut' were comparable in Huh7.5 and they both showed similar replication enhancement in Huh7.5 Ago2 KO cells. Taken all together our data suggest that Ago2 uses viRNAs to downregulate viral replication.

Discussion

The RNAi pathway was originally discovered as an antiviral defense mechanism in plants[56] and later in invertebrates and some vertebrates including mammals.[57] In this study we examined how two critical components of the RNAi pathway affect SARS-CoV-2 infection. Consistent with recent reports,[37,58–60] we found that biogenesis and/or stability of two key cytoplasmic RNA granules associated with RNAi components, SG and P-bodies in infected cells, were disrupted during SARS-CoV-2 infection. In addition, we observed that a pool of Ago2 colocalized with viral replication sites which prompted investigation into how expression of this RNAi effector protein affects SARS-CoV-2 infection. In future studies, it will be of interest to determine which other proteins reside in the Ago2 complexes that associate with viral replication complexes.

Collectively our findings provide strong evidence that Ago2 is a host restriction factor for betacoronaviruses including early (Wuhan-like) and newly emerged variants (Delta and Omicron). In addition, loss of Ago2 resulted in increased replication of the alphacoronavirus 229E suggesting that this host protein has broad spectrum activity against coronaviruses. However, replication of Mayaro virus, an RNA virus belonging to the *Togaviridae* family was unaffected by loss of Ago2 expression. This finding is in agreement with previous studies where Ago2 was found to restrict replication of certain groups of viruses but not others, in plants[61] and mammalian cells.[62]

Mapping studies revealed that the antiviral function of Ago2 requires its endonuclease activity and the ability to bind small RNAs. However, the RNase Dicer, which is necessary for generation of more than 99% of all cellular miRNAs, is not required for the antiviral function of Ago2.[44,63] This observation together with the mutational analyses of Ago2, suggest that while binding of cellular miRNAs to Ago2 is not involved in its restriction factor function, binding to other small RNA species may be central to its antiviral role.

Ago2 binds to a limited number of miRNAs whose biogenesis is independent of Dicer.[20,63] As such, we posit that Ago2 binds virus-derived small siRNAs termed viRNAs that guide Ago2 complexes to viral genomes that are cleaved by the Ago2 endonuclease activity. Mutational studies removing the viRNA CoV2-miR-O7a from the SARS-CoV-2 genome resulted in increased viral titers, mirroring the effect caused by the abrogation of *Ago2* in cells. Intriguingly, infection of *Ago2* KO cells with CoV2-miR-O7a deletion mutant resulted in 10-fold higher viral titers compared to infection with Wuhan WT. This effect was not observed when comparing Delta WT and Delta 7A mut replication in cells lacking Ago2. We posit that in the absence of the only catalytically active Argonaute protein, Ago2, and the absence of the most abundant virus-derived RNA other viRNAs are available for loading onto Ago1, 3 and 4. These other viRNA-Ago complexes facilitate downregulation of host genes involved in the antiviral response. Further research is needed to fully elucidate this effect.

Despite being a determinant for Ago2 restriction, CoV2-miR-O7a is highly conserved among SARS-CoV-2 variants and other betacoronavirusues. It is possible that other functions of CoV2-miR-O7a including targeting host mRNAs including ISGs[53,54] outweigh its detrimental effects on virus

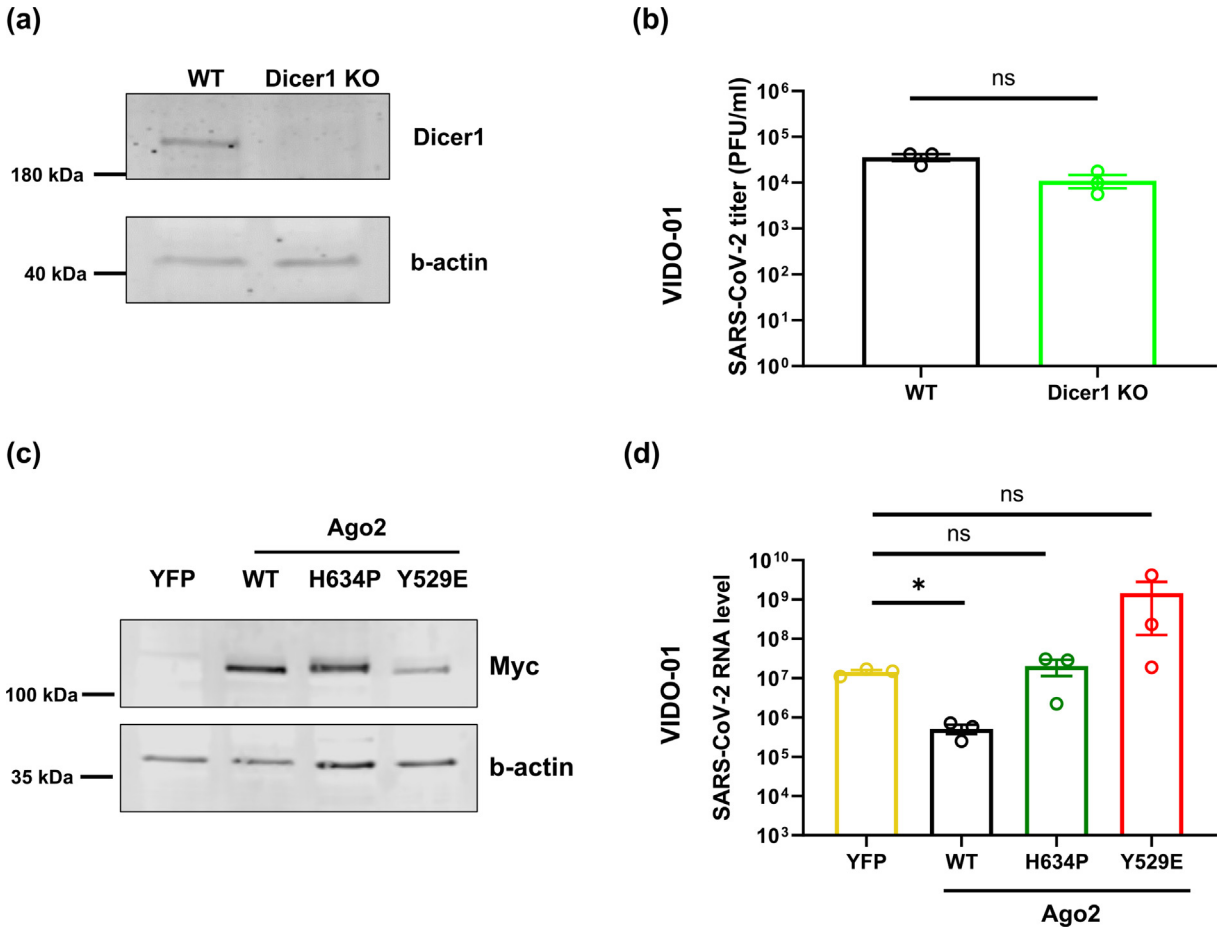

Figure 5. Ago2 endonuclease activity is important for its antiviral function against SARS-CoV-2. (a) Immunoblot analysis of cell lysates from parental (WT) and Huh7.5 *Dicer1* knock-out (KO) by immunoblotting to confirm Dicer1 KO using anti-Dicer1 and anti-actin antibodies. (b) WT and *Dicer1* KO Huh7.5 cells were infected, and viral titers were measured as described in 4b. (c) Huh7.5 Ago2 KO cells were electroporated with plasmids expressing YFP (negative control), Myc-Ago2 wild-type (WT), 3xMyc-Ago2 H634P (lacks endonuclease activity), and Myc-Ago2 Y529E (lacks small RNA binding). Forty-eight hrs post electroporation, cells were lysed and Ago2 expression was evaluated by immunoblotting using anti-myc and anti-actin antibodies. (d) Huh7.5 Ago2 KO cells expressing plasmids encoding Ago2 proteins or control (as described in panel d) were infected with SARS-CoV-2 (MOI = 0.5), and total RNA was harvested 24hpi. Viral RNA level was measured as outlined in Figure 1. Data in figures b and d are from 3 biological replicates. Error bars indicate SEM. Asterisks indicate a statistically significant difference (*$p < 0.05$). Ratio paired t-tests were performed for b. Welch's ANOVA and Dunnett's T3 multiple comparison tests were performed for d.

replication. CoV2-miR-O7a-mediated reduction in replication could also make the virus less lethal to cells, leading to better transmission and increased overall viral fitness. It is unclear how mature CoV2-miR-O7a are produced in infected cells. While a previous study[53] proposed a role for Dicer in the processing of CoV2-miR-O7a, our observation that viral replication is unchanged in *Dicer* knockout cells suggest that processing of this viRNA occurs via a Dicer-independent mechanism similar to that of miR-451.[64] Further studies are required to dissect the molecular mechanisms behind the generation of viRNAs in infected cells.

In summary, ours is the first study to report Ago2 as a potent restriction factor against SARS-CoV-2 and other coronaviruses mediated by viRNAs. Future studies should focus on systematically mapping the viRNAs that are important for Ago2 mediated restriction of coronavirus replication and studying the mechanism behind their biogenesis. In addition, determining whether polymorphisms in the Ago2 gene can be used as biomarkers for disease severity in COVID-19 patients may open new avenues to treat SARS-CoV-2 and potentially other emerging viruses.

Materials and Methods

Cell culture and virus infection. Huh7.5, Huh7.5 Ago2 KO, Calu-3, Vero E6, Vero CCL81,

A549-ACE2 and H23-ACE2 cells were cultured in Dulbecco's modified Eagle's medium (DMEM) (Gibco) supplemented with 100 U/ml penicillin and streptomycin, 1 mM HEPES (Gibco), 2 mM glutamine (Gibco), 10% heat-inactivated fetal bovine serum (FBS) (Gibco) at 37 °C in 5% CO_2.

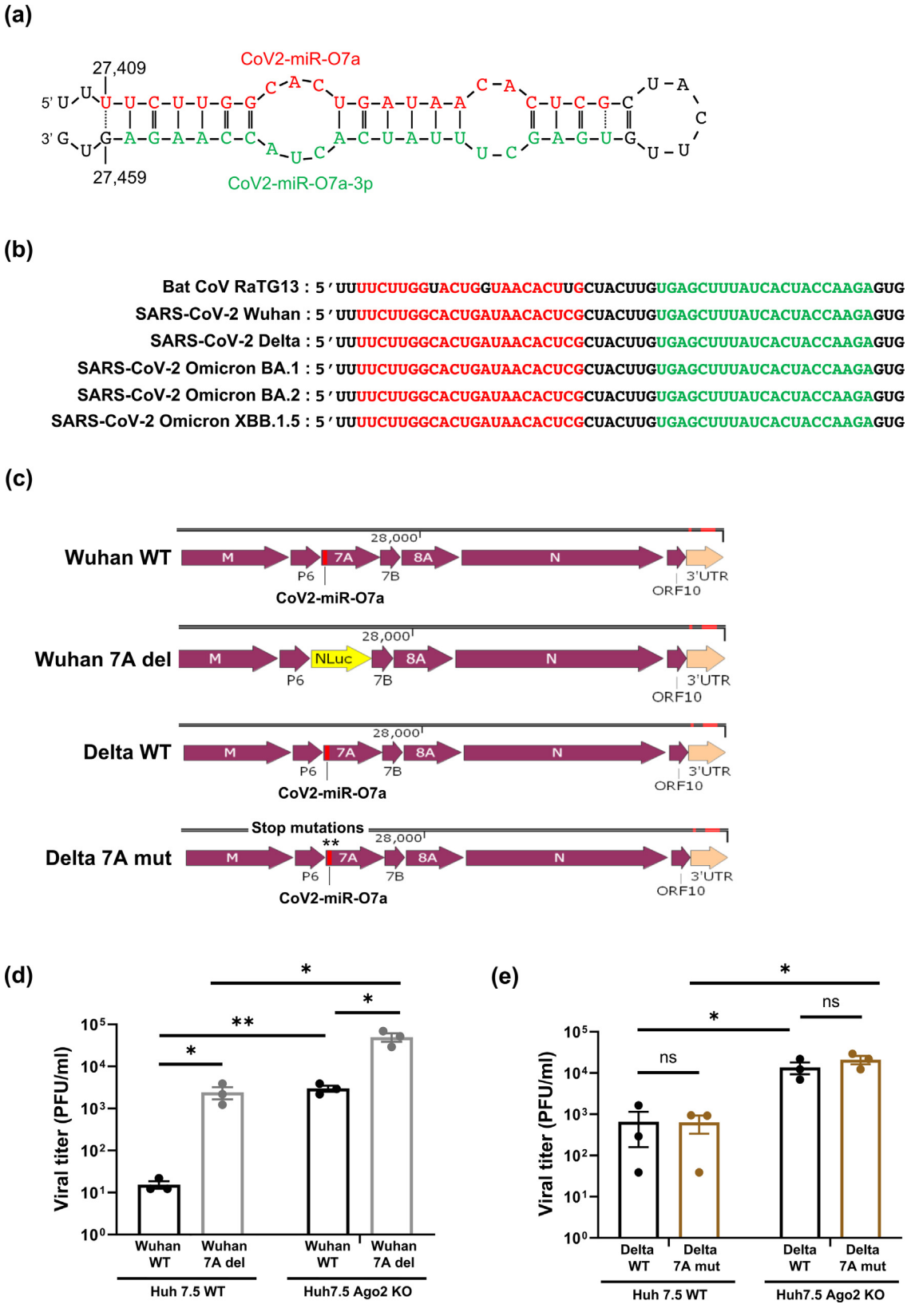

Huh7.5 *Dicer1* KO (kind gift from Charles Rice, Rockefeller University, New York, NY.) were cultured in Dulbecco's modified Eagle's medium (DMEM) (Gibco) supplemented with 100 U/ml penicillin and streptomycin, 1 mM HEPES (Gibco), 2 mM glutamine (Gibco), 20% heat-inactivated fetal bovine serum (FBS) at 37 °C in 5% CO_2. Virus stocks were generated and titrated (by plaque assay) in the following cell lines: SARS-CoV-2 VIDO 01 in Vero E6 cells[14]; SARS-CoV-2 Omicron BA.1 in Vero TMPRSS2 cells; HCoV-229E in Huh7 cells; Mayaro virus in Vero CCL81 cells.

Plasmids, in vitro transcription, electroporation and RNA sequencing. Myc-Ago2 WT construction was described previously.[29] The Ago2 mutant H634P was a kind gift from Dr. G.J. Hannon. Cancer Research UK Cambridge Institute. The Ago2 Y529E mutant was described in.[45] siRNAs against Ago2 (AM16708) and non-targeting control (AM4611) were purchased from Life Technologies. A plasmid encoding the SARS-CoV-2 nucleocapsid gene (N gene) was a gift from Dr. Qiang Liu.[65]

Electroporation was used to introduce plasmid DNA into Huh7.5 and Huh7.5 Ago2 KO cells. Briefly, 1×10^7 cells were resuspended in 1 mL of 25 mM HEPES (pH 7.6), 10 mM KH_2PO_4, 120 mM KCl, 0.15 mM $CaCl_2$, 2 mM ethylene glycol tetra acetic acid (EGTA), 5 mM $MgCl_2$, 5 mM adenosine triphosphate (ATP), and 2 mM l-glutamine. 400 μL of cell suspension and 100 μL of plasmid DNA at 100 ng/μL were used in each electroporation using 4 mm cuvettes (Bio-Rad) at 360 V, 975 μF. siRNAs were transfected using RNAiMax (Life Technologies) following manufacturer's instructions.

The bacmids encoding the T7 promoter driven full length genome of Wuhan wild type (NC_045512 with D614G spike mutation) and Delta wild type (GenBank ID: OU327261.1) were synthesized as cDNA by Telesis Bio. The Wuhan 7A deletion construct was generated by replacing the entire coding sequence of ORF7A with a nanoluciferase gene in the Wuhan wild type backbone without altering the TRS sequence both upstream and downstream of ORF7A. Delta 7A mutant was generated by replacing the coding sequence of the 1st and 12th amino acids (methionine) of ORF7A with stop codons (TAG) in the Delta wild type backbone (Table 2). The construction of Wuhan WT and Nanoluciferase molecular clones and the characterization of the recovered viruses are described here.[55]

The capped genomic RNA from the bacmid clones and the SARS-CoV-2 nucleocapsid-mRNA were generated using mMESSAGE mMACHINE™ T7 Transcription Kit from ThermoFisher Scientific (AM1344) following manufacturer's instructions. The RNAs were purified by phenol: chloroform method followed by isopropanol precipitation. Five micrograms each of viral genomic RNA and N-protein RNA were electroporated into Vero CCL81 cells to recover the infectious virus. The working stocks were generated by amplifying the virus stock once in Vero CCL81 cells. The stocks were titrated by $TCID_{50}$ in Vero CCL81 cells as described,[55] and the integrity of the clones were validated by viral RNA sequencing from total RNA harvested from cells infected with the working stock.

For viral RNA sequencing, Vero CCL81 cells were infected with WT and mutant viruses at 1 MOI and 24 h later, total RNA from cells were harvested using RNeasy Plus mini kit (Qiagen) and cDNA was prepared using Superscript II (ThermoFisher Scientific) and random hexamer primers. ARTIC V4 primer pools (https://github.com/artic-network/artic-ncov2019) were used to generate amplicons using Q5 Hot Start Master Mix (New England Biolabs) with the following PCR program (heat activation 98 °C 30 s, 35 cycles of denaturation 95 °C 15 s, annealing and extension 63 °C 300 s). The PCR products were purified using SPRIselect beads (Beckman Coulter) and the concentration determined using a Qubit fluorometer (ThermoFisher Scientific). The sequencing library was prepared using the Nextera DNA Flex Prep kit (Illumina, USA) according to manufacturer's protocol and paired-end (2×150 bp) sequencing was performed on a MiniSeq with a 300–cycle reagent kit (Illumina, USA). De-multiplexing of sequencing files was done using the native instrument software and the data was analyzed using the Nextflow pipeline for running the ARTIC

Figure 6. viRNA CoV2-miR-O7a is required for Ago2-mediated restriction of target SARS-CoV-2 replication. (a) CoV2-miR-O7a sequence (generated from ORF7A protein coding region) and secondary structure. (b) CoV2-miR-O7a conservation among SARS-CoV-2 variants and other coronaviruses (c) Schematic representation of the SARS-CoV2 molecular clones used (from M gene to 3′ UTR; generated using Snapgene software). Wuhan WT and Delta WT have intact ORF7A coding region. In Wuhan 7A del virus, the ORF7A sequence was swapped with the NanoLuciferase (NLuc) gene abrogating expression of ORF7A protein and CoV2-miR-O7a. In Delta 7A mut virus, the start codon of ORF7A gene was mutated to abolish protein translation without affecting CoV2-miR-O7a. (d-e). Viruses shown in panel c were used to infect WT or *Ago2* KO Huh7.5 cells (MOI = 0.1) after which media were harvested at 24hpi. Viral titers were measured using the $TCID_{50}$ method. Data in figure d and e are from 3 biological replicates. Error bars indicate SEM. Asterisks indicate a statistically significant difference (*$p < 0.05$, **$p < 0.01$). Multiple t-tests using the Holm-Sidak method were performed for d and e.

field bioinformatics tools (https://github.com/jts/ncov2019-artic-nf).

Antibodies and compounds. Commercially available antibodies were purchased from the following sources: Mouse anti-β-actin (A3853) from Sigma-Aldrich (St. Louis, MO); Rabbit anti-dcp1a (ab47811) from Abcam; Goat anti-ACE2 (AF933) from R&D Systems (Minnesota); Goat anti-T-cell-restricted intracellular antigen (TIA-1) (sc-1751) were from Santa Cruz Biotechnology; mouse monoclonal anti-double-strand RNA J2 (10010200) from Scicons (Nordic MUbio), Hungary; Rabbit anti-SARS-CoV-2 nucleocapsid antibody (GTX135357) from GeneTex; Rat anti-Ago2 (11A9), a kind gift from Dr. Gunter Meister, University of Regensburg, Germany; Rabbit anti-c-myc (C3956) Sigma-Aldrich (St. Louis, MO); Donkey anti-rat conjugated to Alexa 647 (A-78947), chicken anti-goat conjugated to Alexa 488 (A-21467), donkey anti-rabbit conjugated to Alexa 568 (A-10042), goat anti-human conjugated to Alexa 488 (A-11013), Donkey anti-mouse conjugated to Alexa 594 (A-11058), Donkey anti-mouse conjugated to Alexa 488 (A-21202), goat anti-rat conjugated to Alexa 680 (A-21096), Donkey anti-rabbit conjugated to Alexa 488 (A-21206) and goat anti-mouse conjugated to Alexa 750 (A-21057) were purchased from Life Technologies. Human anti-GW was a gift from Dr. M. Fritzler (University of Calgary, Calgary, AB, Canada); Rabbit anti SARS-CoV-2 NC (GTX135357) was from GeneTex (Irvine, CA). Mouse monoclonal anti-myc (9E10) was prepared from a hybridoma cell line obtained from the American Type Culture Collection (ATCC). Hippuristanol was prepared in dimethyl sulfoxide (DMSO; Sigma-Aldrich, St. Louis, MO) and stored at −80 °C; Sodium arsenite solution from Sigma Aldrich (St Louis, MO); DAPI dihydrochloride (D9542) was from Sigma-Aldrich (St. Louis, MO).

Immunoblotting. Electroporated Huh7.5, Huh7.5 *Ago2* KO or transfected Calu-3 cells at designated time points post-electroporation or post-transfection, cells were washed twice with phosphate-buffered saline (PBS) before lysing with 2X SDS Sample buffer (62.5 mM Tris-HCl (pH 6.8), 50% (v/v) Glycerol, 2% (w/v) SDS, 0.01% (w/v) Bromophenol blue) with 100 mM dithiothreitol (DTT). Molecular size marker, PageRuler™ Plus Prestained Protein Ladder, 10–250 kDa from ThermoFisher Scientific. The samples were incubated at 98 °C for 10 min to denature proteins which were then separated by SDS-PAGE and transferred to polyvinylidene difluoride (PVDF) membranes for immunoblotting. The membranes were incubated with blocking buffer (5% bovine serum albumin [BSA; Sigma Aldrich] in PBS-0.05% Tween 20) for 30 min before exposure to primary antibodies diluted in blocking buffer for 60 min. Following three washes with PBS-0.05% Tween 20 for 10 min each, the membranes were incubated with secondary antibodies diluted in blocking buffer for 60 min. The membranes were then washed three times with PBS-0.05% Tween 20, once with PBS and then imaged with an Odyssey Infrared Imaging system. Quantification of proteins was performed using Odyssey Image Studio Lite Software Version 5.2.

Confocal immunofluorescence (IF) microscopy. H23-ACE2, A549-ACE2, or Huh7.5 Ago2 KO cells on coverslips were fixed for 10 min at room temperature with 2% electron microscopy grade paraformaldehyde (Electron Microscope Sciences) in PBS and permeabilized with 0.2% Triton X-100 in PBS for 5 min. Following three washes with PBS, the samples were incubated in blocking buffer (5% BSA in PBS) at room temperature for 30 min. Primary antibodies were diluted in blocking buffer and incubated at room temperature for 60 min. After three washes with PBS, samples were incubated with secondary antibodies (1:1000, Invitrogen) in blocking buffer and DAPI (1 μg/mL) for 60 min at room temperature. Coverslips were washed three times with PBS and one time with de-ionised water and mounted on microscope slides using Prolong Gold anti-fade mounting reagent (Life Technologies). Samples were imaged using a DeltaVision Elite Deconvolution microscope equipped with a 60× PlanApo N oil objective. Automated protocols in Volocity 6.2.1 software (PerkinElmer) were developed to quantify stress granules or P-bodies on a per cell basis. Masks for stress granules and P-bodies were generated based on volume (objects less than 0.45 μm^3 or 0.02 μm^3 were excluded from analysis for stress granule or P-body counts, respectively) and fluorescence intensity thresholds. Object-based colocalization protocols were developed using Imaris software x64 version 9.3.0 (Oxford Instruments). First, 3-D objects were created as a mask for Ago2, Dcp1a, and dsRNA fluorescent signal on a per cell basis based on diameter (estimated diameters were 0.5 μm, 0.3 μm, and 0.5 μm for Ago2, Dcp1a, and dsRNA structures) and fluorescence intensity thresholds. 3-D objects found within 0.5 μm or less of one another were then identified as co-locating by the software. The percentage of dsRNA 3-D objects co-located to Ago2 or Dcp1a were calculated as: the number of dsRNA co-located to Ago2 or Dcp1a divided by the total number of dsRNA 3-D objects within a cell multiplied by 100.

Quantitative real time PCR (qRT-PCR). Total RNA was isolated from cells using the RNA NucleoSpin Kit (Machery Nagel) and reverse transcribed using random primers (Invitrogen) and Improm-II reverse transcriptase (Promega) at 42 °C for 1.5 h to generate cDNAs. The cDNAs were diluted 1:5 with water and 5% volume was mixed with the appropriate primers (Integrated DNA

Table 1 Primers used for qRT-PCR.

Target Gene	Primer sequences (5′→3′)
SARS-CoV-2 spike	Fwd: CCTACTAAATTAAATGATCTCTGCTTTACT
	Rev: CAAGCTATAACGCAGCCTGTA
ACTB	Fwd: CCTGGCACCCAGCACAAT
	Rev: GCCGATCCACACGGAGTACT

Table 2 **Sequence of SARS-CoV-2 Delta VOC ORF7A WT and Delta VOC ORF7A mutant.** (CoV2-miR-O7a is highlighted in red color).

Gene	Open reading frame sequence (5'→3')
Delta ORF7A WT	ATGAAAATTATTCTTTTCTTGGCACTGATAACACTCGCTACTTGTGAGCTTTATCACTA CCAAGAGTGTGTTAGAGGTACAACAGTACTTTTAAAAGAACCTTGCTCTTCTGGAAC ATACGAGGGCAATTCACCATTTCATCCTCTAGCTGATAACAAATTTGCACTGACTTGC TTTAGCACTCAATTTGCTTTTGCTTGTCCTGACGGCGTAAAACACGTCTATCAGTTACG TGCCAGATCAGCTTCACCTAAACTGTTCATCAGACAAGAGGAAGTTCAAGAACTTTAC TCTCCAATTTTTCTTATTGTTGCGGCAATAGTGTTTATAACACTTTGCTTCACACTCAA AAGAAAGATAGAATGA
Delta ORF7A Mutant	TAGAAAATTATTCTTTTCTTGGCACTGATATAGCTCGCTACTTGTGAGCTTTATCACTA CCAAGAGTGTGTTAGAGGTACAACAGTACTTTTAAAAGAACCTTGCTCTTCTGGAAC ATACGAGGGCAATTCACCATTTCATCCTCTAGCTGATAACAAATTTGCACTGACTTGC TTTAGCACTCAATTTGCTTTTGCTTGTCCTGACGGCGTAAAACACGTCTATCAGTTACG TGCCAGATCAGCTTCACCTAAACTGTTCATCAGACAAGAGGAAGTTCAAGAACTTTAC TCTCCAATTTTTCTTATTGTTGCGGCAATAGTGTTTATAACACTTTGCTTCACACTCAA AAGAAAGATAGAATGA

Technologies) and the PerfecTa SYBR green SuperMix with Low ROX (Quanta Biosciences) and amplified for 40 cycles (30 s at 94 °C, 40 s at 55 °C and 20 s at 68 °C) in a Biorad CFX96 qRT-PCR machine. The gene targets and primer sequence are listed in Table 1. The CT values were normalized using *Actb* mRNA as the internal control or by cell count. The ΔΔCT values were determined using control samples as the reference value. Relative levels of mRNAs were calculated using the formulas $2^{(-\Delta\Delta CT)}$.

Statistical analyses. All statistical analyses were performed using GraphPad Prism software.

DATA AVAILABILITY

Data will be made available on request.

DECLARATION OF COMPETING INTEREST

The authors declare that they have no known competing financial interests or personal relationships that could have appeared to influence the work reported in this paper.

Acknowledgements

This work was funded by the grants from the Canadian Institutes of Health Research (OV3-172302; GA1-177707) to T.C.H. and (PUU-177963; PTT-179810; MM1 181121) to A.K. and T.C.H, and (VR3-172626) to J.A.W. J.A.W also acknowledges membership in, and funding from CIHR operating grant to the Coronavirus Variants Rapid Response Network (CoVaRR-Net) (FRN# 175622). SARS-CoV-2 research in the laboratory of D.F. is supported by the CIHR grants OV5-170349, VRI-173022 and VS1-175531. The T.C.H. lab also acknowledges funding from the Natural Sciences and Engineering Research Council. VIDO receives operational support from the Province of Saskatchewan through Innovation Saskatchewan and the Canadian Foundation for Innovation through the Major Science Initiatives.

The funders had no role in study design, data collection and interpretation, or decision to submit the work for publication.

J.L.-O., N.F., T.C.H, and A.K. conceived the research and drafted the manuscript. J.L.-O., N.F., J.K., A.F.-L., M.E., M.R., M.S. and A.K. carried out the experiments. J.L.-O., and N.F. created the

figures. All authors discussed the results and contributed to the revision of the final manuscript.

The authors thank V. Mancinelli and E. Reklow for technical support. The authors acknowledge the services of the University of Alberta Faculty of Medicine & Dentistry Cell Imaging Centre core facility, and VIDO at the University of Saskatchewan for their services used in this study.

Appendix A. Supplementary data

Supplementary data to this article can be found online at https://doi.org/10.1016/j.jmb.2023.168170.

Received 10 October 2022;
Accepted 30 May 2023;
Available online xxxx

Keywords:
innate immunity;
coronaviruses;
viral microRNAs;
RNAi;
Ago_2

† These authors contributed equally to this work.

References

1. Zhou, P., Yang, X.L., Wang, X.G., Hu, B., Zhang, L., Zhang, W., et al., (2020). A pneumonia outbreak associated with a new coronavirus of probable bat origin. *Nature* **579**, 270–273.
2. Guo, L., Wang, M., Zhang, L., Mao, N., An, C., Xu, L., et al., (2021). Transmission risk of viruses in large mucosalivary droplets on the surface of objects: a time-based analysis. *Infect. Dis. Now.* **51**, 219–227.
3. Kohanski, M.A., Lo, L.J., Waring, M.S., (2020). Review of indoor aerosol generation, transport, and control in the context of COVID-19. *Int. Forum Allergy Rhinol.* **10**, 1173–1179.
4. Meyerowitz, E.A., Richterman, A., Gandhi, R.T., Sax, P.E., (2021). Transmission of SARS-CoV-2: a review of viral, host, and environmental factors. *Ann. Intern. Med.* **174**, 69–79.
5. Forchette, L., Sebastian, W., Liu, T., (2021). A comprehensive review of COVID-19 virology, vaccines, variants, and therapeutics. *Curr. Med. Sci.* **41**, 1037–1051.
6. Couzin-Frankel, J., (2021). Antiviral pills could change pandemic's course. *Science* **374**, 799–800.
7. Fiolet, T., Kherabi, Y., MacDonald, C.J., Ghosn, J., Peiffer-Smadja, N., (2022). Comparing COVID-19 vaccines for their characteristics, efficacy and effectiveness against SARS-CoV-2 and variants of concern: a narrative review. *Clin. Microbiol. Infect.* **28**, 202–221.
8. Tao, K., Tzou, P.L., Nouhin, J., Gupta, R.K., de Oliveira, T., Kosakovsky Pond, S.L., et al., (2021). The biological and clinical significance of emerging SARS-CoV-2 variants. *Nature Rev. Genet.* **22**, 757–773.
9. Gordon, D.E., Jang, G.M., Bouhaddou, M., Xu, J., Obernier, K., White, K.M., et al., (2020). A SARS-CoV-2 protein interaction map reveals targets for drug repurposing. *Nature* **583**, 459–468.
10. Gordon, D.E., Hiatt, J., Bouhaddou, M., Rezelj, V.V., Ulferts, S., Braberg, H., et al., (2020). Comparative host-coronavirus protein interaction networks reveal pan-viral disease mechanisms. *Science* **370**
11. Wang, R., Simoneau, C.R., Kulsuptrakul, J., Bouhaddou, M., Travisano, K.A., Hayashi, J.M., et al., (2021). Genetic screens identify host factors for SARS-CoV-2 and common cold coronaviruses. *Cell* **184**, 106–119.e14.
12. White, J.M., Schiffer, J.T., Bender Ignacio, R.A., Xu, S., Kainov, D., Ianevski, A., et al., (2021). Drug combinations as a first line of defense against coronaviruses and other emerging viruses. *mBio* **12**, e0334721
13. Lokugamage, K.G., Hage, A., de Vries, M., Valero-Jimenez, A.M., Schindewolf, C., Dittmann, M., et al., (2020). Type I interferon susceptibility distinguishes SARS-CoV-2 from SARS-CoV. *J. Virol.* **94**
14. Kumar, A., Ishida, R., Strilets, T., Cole, J., Lopez-Orozco, J., Fayad, N., et al., (2021). SARS-CoV-2 nonstructural protein 1 inhibits the interferon response by causing depletion of key host signaling factors. *J. Virol.* **95**, e0026621.
15. Hannon, G.J., (2002). RNA interference. *Nature* **418**, 244–251.
16. Ding, S.W., Voinnet, O., (2007). Antiviral immunity directed by small RNAs. *Cell* **130**, 413–426.
17. Kemp, C., Mueller, S., Goto, A., Barbier, V., Paro, S., Bonnay, F., et al., (2013). Broad RNA interference-mediated antiviral immunity and virus-specific inducible responses in Drosophila. *J. Immunol.* **190**, 650–658.
18. Sarkies, P., Miska, E.A., (2013). RNAi pathways in the recognition of foreign RNA: antiviral responses and host-parasite interactions in nematodes. *Biochem. Soc. Trans.* **41**, 876–880.
19. tenOever, B.R., (2016). The evolution of antiviral defense systems. *Cell Host Microbe* **19**, 142–149.
20. Herrera-Carrillo, E., Berkhout, B., (2017). Dicer-independent processing of small RNA duplexes: mechanistic insights and applications. *Nucleic Acids Res.* **45**, 10369–10379.
21. Li, Y., Basavappa, M., Lu, J., Dong, S., Cronkite, D.A., Prior, J.T., et al., (2016). Induction and suppression of antiviral RNA interference by influenza A virus in mammalian cells. *Nature Microbiol.* **2**, 16250.
22. Cui, L., Wang, H., Ji, Y., Yang, J., Xu, S., Huang, X., et al., (2015). The nucleocapsid protein of coronaviruses acts as a viral suppressor of RNA silencing in mammalian cells. *J. Virol.* **89**, 9029–9043.
23. Mukhopadhyay, U., Chanda, S., Patra, U., Mukherjee, A., Komoto, S., Chawla-Sarkar, M., (2019). Biphasic regulation of RNA interference during rotavirus infection by modulation of Argonaute2. *Cell. Microbiol.* **21**, e13101.
24. Wilson, J.A., Zhang, C., Huys, A., Richardson, C.D., (2011). Human Ago2 is required for efficient microRNA 122 regulation of hepatitis C virus RNA accumulation and translation. *J. Virol.* **85**, 2342–2350.
25. Eckenfelder, A., Ségéral, E., Pinzón, N., Ulveling, D., Amadori, C., Charpentier, M., et al., (2017). Argonaute proteins regulate HIV-1 multiply spliced RNA and viral production in a Dicer independent manner. *Nucleic Acids Res.* **45**, 4158–4173.
26. Madsen, C., Hooper, I., Lundberg, L., Shafagati, N., Johnson, A., Senina, S., et al., (2014). Small molecule

inhibitors of Ago2 decrease Venezuelan equine encephalitis virus replication. *Antiviral Res.* **112**, 26–37.
27. Liu, J., Carmell, M.A., Rivas, F.V., Marsden, C.G., Thomson, J.M., Song, J.J., et al., (2004). Argonaute2 is the catalytic engine of mammalian RNAi. *Science* **305**, 1437–1441.
28. Meister, G., Landthaler, M., Patkaniowska, A., Dorsett, Y., Teng, G., Tuschl, T., (2004). Human Argonaute2 mediates RNA cleavage targeted by miRNAs and siRNAs. *Mol. Cell* **15**, 185–197.
29. Pare, J.M., Tahbaz, N., López-Orozco, J., LaPointe, P., Lasko, P., Hobman, T.C., (2009). Hsp90 regulates the function of argonaute 2 and its recruitment to stress granules and P-bodies. *Mol. Biol. Cell* **20**, 3273–3284.
30. Liu, J., Valencia-Sanchez, M.A., Hannon, G.J., Parker, R., (2005). MicroRNA-dependent localization of targeted mRNAs to mammalian P-bodies. *Nature Cell Biol.* **7**, 719–723.
31. Jackson, C.B., Farzan, M., Chen, B., Choe, H., (2022). Mechanisms of SARS-CoV-2 entry into cells. *Nature Rev. Mol. Cell Biol.* **23**, 3–20.
32. Ostrov, D.A., Bluhm, A.P., Li, D., Khan, J.Q., Rohamare, M., Rajamanickam, K., et al., (2021). Highly specific sigma receptor ligands exhibit anti-viral properties in SARS-CoV-2 infected cells. *Pathogens*, 10.
33. Collier, N.C., Schlesinger, M.J., (1986). The dynamic state of heat shock proteins in chicken embryo fibroblasts. *J. Cell Biol.* **103**, 1495–1507.
34. Chaudhry, Y., Nayak, A., Bordeleau, M.E., Tanaka, J., Pelletier, J., Belsham, G.J., et al., (2006). Caliciviruses differ in their functional requirements for eIF4F components. *J. Biol. Chem.* **281**, 25315–25325.
35. Liu, J., Rivas, F.V., Wohlschlegel, J., Yates, J.R., Parker, R., Hannon, G.J., (2005). A role for the P-body component GW182 in microRNA function. *Nature Cell Biol.* **7**, 1261–1266.
36. Jakymiw, A., Lian, S., Eystathioy, T., Li, S., Satoh, M., Hamel, J.C., et al., (2005). Disruption of GW bodies impairs mammalian RNA interference. *Nature Cell Biol.* **7**, 1267–1274.
37. Kleer, M., Mulloy, R.P., Robinson, C.A., Evseev, D., Bui-Marinos, M.P., Castle, E.L., et al., (2022). Human coronaviruses disassemble processing bodies. *PLoS Pathog.* **18**, e1010724.
38. Gaete-Argel, A., Marquez, C.L., Barriga, G.P., Soto-Rifo, R., Valiente-Echeverria, F., (2019). Strategies for success. Viral infections and membraneless organelles. *Front. Cell Infect. Microbiol.* **9**, 336.
39. McCormick, C., Khaperskyy, D.A., (2017). Translation inhibition and stress granules in the antiviral immune response. *Nature Rev. Immunol.* **17**, 647–660.
40. Gao, B., Gong, X., Fang, S., Weng, W., Wang, H., Chu, H., et al., (2021). Inhibition of anti-viral stress granule formation by coronavirus endoribonuclease nsp15 ensures efficient virus replication. *PLoS Pathog.* **17**, e1008690.
41. Amador-Cañizares, Y., Panigrahi, M., Huys, A., Kunden, R. D., Adams, H.M., Schinold, M.J., et al., (2018). miR-122, small RNA annealing and sequence mutations alter the predicted structure of the Hepatitis C virus 5' UTR RNA to stabilize and promote viral RNA accumulation. *Nucleic Acids Res.* **46**, 9776–9792.
42. Saccon, E., Chen, X., Mikaeloff, F., Rodriguez, J. E., Szekely, L., Vinhas, B.S., et al., (2021). Cell-type-resolved quantitative proteomics map of interferon response against SARS-CoV-2. *iScience* **24**, 102420
43. Yu, Y., Scheel, T.K.H., Luna, J.M., Chung, H., Nishiuchi, E., Scull, M.A., et al., (2017). miRNA independent hepacivirus variants suggest a strong evolutionary pressure to maintain miR-122 dependence. *PLoS Pathog.* **13**, e1006694
44. Kim, Y.K., Kim, B., Kim, V.N., (2016). Re-evaluation of the roles of DROSHA, Export in 5, and DICER in microRNA biogenesis. *PNAS* **113**, E1881–E1889.
45. Lopez-Orozco, J., Pare, J.M., Holme, A.L., Chaulk, S.G., Fahlman, R.P., Hobman, T.C., (2015). Functional analyses of phosphorylation events in human Argonaute 2. *RNA* **21**, 2030–2038.
46. Rudel, S., Wang, Y., Lenobel, R., Korner, R., Hsiao, H.H., Urlaub, H., et al., (2011). Phosphorylation of human Argonaute proteins affects small RNA binding. *Nucleic Acids Res.* **39**, 2330–2343.
47. Parameswaran, P., Sklan, E., Wilkins, C., Burgon, T., Samuel, M.A., Lu, R., et al., (2010). Six RNA viruses and forty-one hosts: viral small RNAs and modulation of small RNA repertoires in vertebrate and invertebrate systems. *PLoS Pathog.* **6**, e1000764.
48. Girardi, E., Lefèvre, M., Chane-Woon-Ming, B., Paro, S., Claydon, B., Imler, J.L., et al., (2015). Cross-species comparative analysis of Dicer proteins during Sindbis virus infection. *Sci. Rep.* **5**, 10693.
49. Backes, S., Langlois, R.A., Schmid, S., Varble, A., Shim, J. V., Sachs, D., et al., (2014). The Mammalian response to virus infection is independent of small RNA silencing. *Cell Rep.* **8**, 114–125.
50. Bogerd, H.P., Skalsky, R.L., Kennedy, E.M., Furuse, Y., Whisnant, A.W., Flores, O., et al., (2014). Replication of many human viruses is refractory to inhibition by endogenous cellular microRNAs. *J. Virol.* **88**, 8065–8076.
51. Maillard, P.V., Ciaudo, C., Marchais, A., Li, Y., Jay, F., Ding, S.W., et al., (2013). Antiviral RNA interference in mammalian cells. *Science* **342**, 235–238.
52. Meng, F., Siu, G.K., Mok, B.W., Sun, J., Fung, K.S.C., Lam, J.Y., et al., (2021). Viral microRNAs encoded by nucleocapsid gene of SARS-CoV-2 are detected during infection, and targeting metabolic pathways in host cells. *Cells.*, 10.
53. Singh, M., Chazal, M., Quarato, P., Bourdon, L., Malabat, C., Vallet, T., et al., (2022). A virus-derived microRNA targets immune response genes during SARS-CoV-2 infection. *EMBO Rep.* **23**, e54341.
54. Pawlica, P., Yario, T.A., White, S., Wang, J., Moss, W.N., Hui, P., et al., (2021). SARS-CoV-2 expresses a microRNA-like small RNA able to selectively repress host genes. *PNAS* **118**
55. Juveriya Qamar, K., Megha, R., Karthic, R., Kalpana, K.B., Jocelyne, L., Anil, K., et al., (2023). Generation of a SARS-CoV-2 reverse genetics system and novel human lung cell lines that exhibit high virus-induced cytopathology. *bioRxiv.* 2023:2023.03.08.531833.
56. Hamilton, A.J., Baulcombe, D.C., (1999). A species of small antisense RNA in posttranscriptional gene silencing in plants. *Science* **286**, 950–952.
57. Obbard, D.J., Gordon, K.H., Buck, A.H., Jiggins, F.M., (2009). The evolution of RNAi as a defence against viruses and transposable elements. *Philos. Trans. R. Soc. London B Biol. Sci.* **364**, 99–115.

58. Kim, D., Maharjan, S., Kang, M., Kim, J., Park, S., Kim, M., et al., (2022). Differential effect of SARS-CoV-2 infection on stress granule formation in Vero and Calu-3 cells. *Front. Microbiol.* **13**, 997539
59. Zheng, Z.Q., Wang, S.Y., Xu, Z.S., Fu, Y.Z., Wang, Y.Y., (2021). SARS-CoV-2 nucleocapsid protein impairs stress granule formation to promote viral replication. *Cell Discov.* **7**, 38.
60. Liu, H., Bai, Y., Zhang, X., Gao, T., Liu, Y., Li, E., et al., (2022). SARS-CoV-2 N protein antagonizes stress granule assembly and IFN production by interacting with G3BPs to facilitate viral replication. *J. Virol.* **96**, e0041222.
61. Ludman, M., Burgyán, J., Fátyol, K., (2017). Crispr/Cas9 mediated inactivation of argonaute 2 reveals its differential involvement in antiviral responses. *Sci. Rep.* **7**, 1010.
62. Schuster, S., Overheul, G.J., Bauer, L., van Kuppeveld, F. J.M., van Rij, R.P., (2019). No evidence for viral small RNA production and antiviral function of Argonaute 2 in human cells. *Sci. Rep.* **9**, 13752.
63. Liu, Y.P., Schopman, N.C., Berkhout, B., (2013). Dicer-independent processing of short hairpin RNAs. *Nucleic Acids Res.* **41**, 3723–3733.
64. Cheloufi, S., Dos Santos, C.O., Chong, M.M., Hannon, G. J., (2010). A dicer-independent miRNA biogenesis pathway that requires Ago catalysis. *Nature* **465**, 584–589.
65. Nguyen, H.T., Falzarano, D., Gerdts, V., Liu, Q., (2021). Construction of a noninfectious SARS-CoV-2 replicon for antiviral-drug testing and gene function studies. *J. Virol.* **95**, e00687–e721.